The Institution of
Engineering and Technology WILEY

ORIGINAL RESEARCH

Preparation and characterisation of ciprofloxacin-loaded silver nanoparticles for drug delivery

Samer Hasan Hussein-Al-Ali[1,2] 🆔 | Suha Mujahed Abudoleh[1] |
Qais Ibrahim Abdallah Abualassal[1] | Zead Abudayeh[1] | Yousef Aldalahmah[1] |
Mohd Zobir Hussein[3]

[1]Faculty of Pharmacy, Isra University, Amman, Jordan

[2]Department of Chemistry, Faculty of Science, Isra University, Amman, Jordan

[3]Materials Synthesis and Characterization Laboratory, Institute of Advanced Technology (ITMA), University Putra Malaysia, Serdang, Selangor, Malaysia

Correspondence

Samer Hasan Hussein-Al-Ali, Faculty of Pharmacy, Isra University, P.O. Box 22, Amman 11622, Jordan.
Email: sameralali72@yahoo.com and samer.alali@iu.edu.jo

Funding information

Faculty of Pharmacy at Isra University, and University Putra Malaysia, Grant/Award Number: 9443100 NANOMITE

Abstract

Silver nanoparticles (AgNPs) have shown potential applications in drug delivery. In this study, the AgNPs was prepared from silver nitrate in the presence of alginate as a capping agent. The ciprofloxacin (Cipro) was loaded on the surface of AgNPs to produce Cipro-AgNPs nanocomposite. The characteristics of the Cipro-AgNPs nanocomposite were studied by X-ray diffraction (XRD), UV–Vis, transmission electron microscopy (TEM), thermogravimetric analysis (TGA), scanning electron microscopy (SEM), Fourier-transform infra-red analysis (FT-IR) and zeta potential analyses. The XRD of AgNPs and Cipro-AgNPs nanocomposite data showed that both have a crystalline structure in nature. The FT-IR data indicate that the AgNPs have been wrapped by the alginate and loaded with the Cipro drug. The TEM image showed that the Cipro-AgNPs nano-composites have an average size of 96 nm with a spherical shape. The SEM image for AgNPs and Cipro-AgNPs nanocomposites confirmed the needle-lumpy shape. The zeta potential for Cipro-AgNPs nanocomposites exhibited a positive charge with a value of 6.5 mV. The TGA for Cipro-AgNPs nanocomposites showed loss of 79.7% in total mass compared to 57.6% for AgNPs which is due to the Cipro loaded in the AgNPs. The release of Cipro from Cipro-AgNPs nanocomposites showed slow release properties which reached 98% release within 750 min, and followed the Hixson–Crowell kinetic model. In addition, the toxicity of AgNPs and Cipro-AgNPs nanocomposites was evaluated using normal (3T3) cell line. The present work suggests that Cipro-AgNPs are suitable for drug delivery.

KEYWORDS

ciprofloxacin, cytotoxicity, nanocomposite, silver nanoparticles, slow release

1 | INTRODUCTION

A short time ago, nanomaterials became one of the most exciting research areas in drug delivery. They have several desirable physicochemical properties like small size and large surface [1]. In fact, nanomaterials applications have been utilised in different fields, for example, immunology [2], antimicrobial studies [3], drug solubility, bioavailability, and pulmonary system studies [4].

Preparation of metal nanoparticles is executed by different methods, such as pyrolysis [5], sol–gel [6], and chemical vapor deposition [7]. Silver nanoparticles (AgNPs) are one example of these metal nanoparticles. AgNPs have been the target of study for 10 years due to their novel properties, which make them useful to biomedical applications [8].

A simple preparation method for AgNPs was called the green method, which was dependable, rapid, and non-toxic [9]. A few researchers tried to incorporate AgNPs with

liposomes, hydrogel beads, nanoemulsions and cyclodextrins, in an attempt to achieve targeted delivery, lower toxicity and better compatibility [10, 11]. For example, preparation of AgNPs-liposomes has shown enhanced antibacterial activity, dermal delivery and stability properties compared to AgNPs alone [11]. Another study found that interaction of β-cyclodextrins with AgNPs enhanced the catalytic activity [12].

AgNPs are one of the nanoparticles that have been used as drug delivery carriers [13–15]. The studies propose that AgNPs can carry drugs to their target which enhances therapeutic properties; moreover, synergism between AgNPs and antibiotics drugs occurs which increases their antibacterial properties. These suppositions have been evaluated by different researchers; for example, conjugation of AgNPs with tetracycline or vancomycin and azathioprine [13–15].

Ciprofloxacin (Cipro) is a fluoroquinolone antibiotic used to treat diseases caused by both Gram-positive and Gram-negative bacteria, including *Staphylococcus* spp. And *Pseudomonas* spp. [16] and it was developed in 1981 by Bayer [17]. Cipro is able to bind to bacterial DNA gyrase and therefore inhibit DNA replication. It is rarely soluble in methylene chloride and ethanol, and insoluble in water [18]. Poorly water-soluble drugs usually need high doses in order to maintain the drug concentration in plasma at constant levels after administration. Low aqueous solubility of the drug is the main problem in drug formulations [19].

Drug insolubility can be avoided by nanoformulations of the drug, which include liposomes, micro-particles, micelles, polymeric nanoparticles, and nanosuspension [20–23]. The bioavailability of Cipro can be improved by preparation of new formulations.

Cipro-single-walled carbon nanotubes show significant antibacterial activity towards *Escherichia coli*, *Pseudomonas aeruginosa* and *Staphylococcus aureus*, compared with free Cipro [24].

Conjugation of Cipro-gold nanoparticles show more efficiency towards Gram-negative bacteria when compared with Gram-positive bacteria. This is due to the interaction of the nanoparticles with PO_4^{-3}/NH_3 groups of the outer membrane of Gram-negative bacterial cell walls [25].

In addition, Cipro nano-niosomes show high intracellular antimicrobial activities. Therefore, this product is suitable for drug delivery with high efficacy and safety properties [26].

Cipro-loaded poly-ε-caprolactone nanoparticles were prepared for pulmonary use. The study showed inhibited growth of bacteria. These results indicated that nanoparticles can be used for pulmonary delivery [27].

Therefore, the major aim of this fundamental research is to prepare new nanocomposites as a drug delivery system, using Cipro as an insoluble medication. The nanocomposites have been characterized in terms of size, charge, surface morphology, thermal analysis, release kinetics, drug release, and the cytotoxicity of the nanocomposites.

2 | MATERIALS, METHODS AND CHARACTERIZATION

2.1 | Materials

Cipro (97% purity), sodium alginate polymer (molecular weight ∼500,000 Da) and silver nitrate, phosphate buffer tablet, MTT, and Dulbecco's Modified Eagle medium (DMEM) were purchased from Sigma-Aldrich. Mouse embryonic fibroblast cells (3T3) were purchased from the American Type Culture Collection. obtained from Sigma Aldrich.

2.2 | Preparation of silver nanoparticles (AgNPs)

The solution of sodium alginate was prepared by dissolving 1.5 wt.% into 100 ml of deionised water. Then, a 0.05 M/50 ml of an aqueous silver nitrate solution was dropped into the sodium alginate solution with magnetic stirring. The pH of the prepared solution was adjusted using 0.1 M sodium hydroxide. The suspension immediately turned to a dark brown colour, leading to the formation of AgNPs. The component was continuously stirred for 30 min and the obtained suspensions of AgNPs were washed and centrifuged at 11,000 rpm. The AgNPs powder was kept for further use (Scheme A).
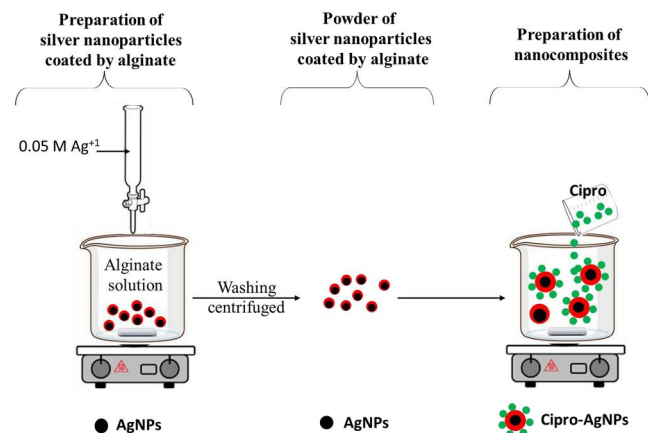
2.3 | Preparation of the Cipro-AgNPs nanocomposite

Typically, 0.6 gm of Cipro was added to 50 ml water. The Cipro-AgNPs nanocomposite was prepared by mixing a solution of Cipro with a known weight of AgNPs (0.1 gm/50 ml). The product was magnetically stirred for 18 h to facilitate Cipro uptake. The nanocomposites were collected using centrifugation, and then washed five times using deionised water. These were denoted as Cipro-AgNPs nanocomposites (Scheme A).

2.4 | UV–VIS spectrophotometer analysis for Cipro quantities loaded and released from Cipro-AgNPs nanocomposite

UV–VIS spectra for Cipro were determined using the double beam UV/Visible spectrophotometer (Shimadzu UV-1601) at λ_{max} 276 nm.

Cipro release profiles from the Cipro-AgNPs nanocomposites were determined using phosphate buffer at pH 7.4. Around 200 mg of the Cipro-AgNPs nanocomposite was placed into the dissolution apparatus containing 500 ml of release media. The cumulative concentration of Cipro released from the nanocomposites in media was determined at different times at $\lambda_{max} = 276$ nm.

S C H E M E A Representation of silver nanoparticles (AgNPs) and Cipro-AgNPs nanocomposites

The loading of Cipro in Cipro-AgNPs was determined using the supernatant produced from the preparation of nanocomposites. A 2.0 ml aliquot of the supernatant was centrifuged (Hettich Universal 30 RF) at 11,000 rpm for 20 min. Finally, the unbound Cipro was determined by the UV/Visible spectrophotometer at λ_{max} 276 nm. The % loading was calculated as follows:

$$\% \text{ Loading} = \frac{C_T - C_{un}}{\text{mass of nanocomposite}} \times 100 \quad (1)$$

where C_T is the Cipro concentration used during preparation of the nanocomposites, and C_{un} is the unbound Cipro in the solution.

2.5 | X-ray diffraction (XRD)

XRD is a good method used for characterising the crystallinity of materials and it provides information on structures. In this work, XRD was used to study the structure of the AgNPs and Cipro-AgNPs nanocomposites in the $2\theta = 30°$–$85°$ on an XRD-6000 diffractometer with technical properties of 30 kV and 30 Ma and CuK radiation (λ 1.5406 Å).

2.6 | Fourier-transform infra-red analysis (FT-IR)

FT-IR analysis was used in this work to study the functional groups of the Cipro-AgNPs nanocomposite using Perkin Elmer (model Smart UAIR-two). For this purpose, FT-IR spectra of the AgNPs and Cipro-AgNPs nanocomposite were determined in 4 cm^{-1} resolutions and in the range of 400–4000 cm^{-1}.

2.7 | Thermogravimetric analysis (TGA)

TGA is one technical type of thermal analysis in which the mass is lost during temperature changes. It provides

information about chemical phenomena including thermal decomposition. In this work, TGA analysis was carried out using a Metter-Toledo 851e instrument with the following technical properties (range of 30–900°C, 150 μL alumina crucibles and heating rate of 10°C/min).

2.8 | Zeta potential of nanocomposite

Dynamic light scattering (DLS) with Zetasizer Nano S was used to study the zeta potential of the nanocomposite.

2.9 | Scanning electron microscopy (SEM) for surface morphology of nanocomposites

SEM technique was used to study the surface morphology of the Cipro-AgNPs nanocomposites using a NOVA™ Nano SEM 230 (FEI).

2.10 | Transmission electron microscopy (TEM)

The TEM images were obtained using Hitachi H-7100 and operating at 80 and 200 kV acceleration.

2.11 | Cell culturing and MTT cytotoxicity assay

The MTT assay was applied on the 3T3-L1 cell lines, which are derived from mouse 3T3 cells. The cytotoxicity of Cipro, AgNPs, and Cipro-AgNPs nanocomposites was determined. The 3T3-L1 cells were seeded in 96-well culture plates (1×10^5 cells/well) and cultured in Dulbecco's Modified Eagle Medium containing 10% foetal bovine serum, 15 mmol/ml glutamine, 100 μg/ml streptomycin and 100 unit's/mL penicillin.

A 0.05% concentration of the reagent was added to 3T3 cells. After that, the reagent was replaced with dimethyl sulfoxide for 10 min to solubilise the purple crystals formed. Optical density reading was measured at a wavelength of 570 nm. The percentage of cell viability was estimated according to the literature [28].

3 | RESULTS AND DISCUSSION

3.1 | X-ray diffraction (XRD)

Analysis of the crystal structure for the synthesised AgNPs was achieved by XRD. The XRD analysis of the prepared AgNPs showed diffraction peaks with corresponding planes at $2\theta = 38.4°(111)$, $44.4°$ (200), $64.5°$ (220), $77.7°$ (311) and $81.6°$ (222) [29]. The highest peak in Figure 1a was at $2\theta = 38.4°$ which indicated the silver structure, similar to the results obtained by Roy et al. [30].

Comparative analysis of the XRD spectra for Cipro-AgNPs nanocomposites with the AgNPs confirmed that the synthesised Cipro-AgNPs nanocomposites had the same structure, evident by the peaks with corresponding planes at 2θ values of 38.2° (111), 44.2° (200), 64.5° (220), 77.5° (311) and 81.5° (222) (Figure 1b).

The Scherrer's equation can be used to calculate the size of the AgNPs and Cipro-AgNPs nanocomposite Equation (1), by using the Full Width at Half Maximum (FWHM). Due to the crystalline and cubic nature of the AgNPs, the Scherrer's constant value was selected at 0.94 [31]. The average sizes of the AgNPs and Cipro-AgNPs nanocomposites were found to be 85 nm and 100 nm, respectively.

$$L = \frac{0.94\,\lambda}{\beta \cos \Theta} \qquad (2)$$

where β is in the radian unit and represents the broadening at half of its maximum intensity, λ is the X-ray wavelength (1.5418 Å), and θ is Bragg diffraction angle (in degrees).

3.2 | Infrared spectroscopy (FT-IR)

FT-IR spectra for free Cipro, AgNPs and Cipro-AgNPs nanocomposites were determined in the range between 450 and 4000 cm^{-1} as seen in Figure 2. The FT-IR spectrum of free Cipro shows one strong peak at 3527 cm^{-1} which was due to hydroxide stretching. A band at 2937 cm^{-1} represented C–H cyclo alkane, aromatic C-H stretching, and aromatic C = C stretching vibration. The peak at 1702 cm^{-1} represented

carbonyl stretching of the carboxylic group, while the peak at 1622 cm^{-1} was assigned to stretching of the carbonyl group of quinolones. The peak at 1439 cm^{-1} represented stretching of
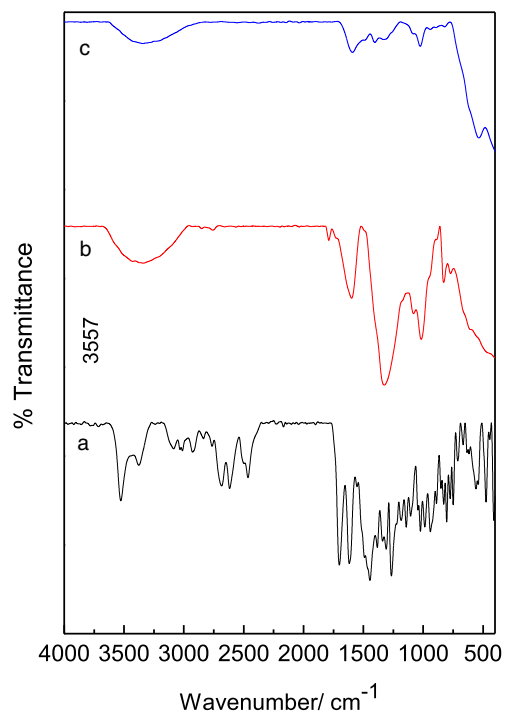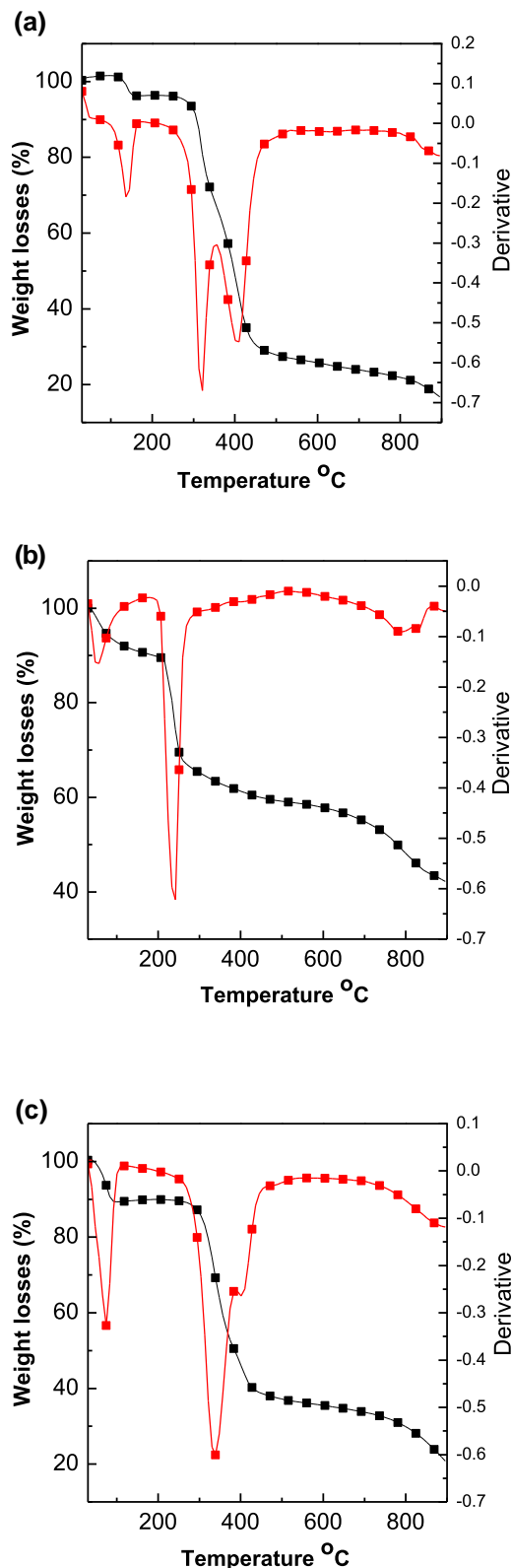

FIGURE 2 FT-IR spectra of the free Cipro (a), silver nanoparticles (AgNPs) (b) and Cipro-AgNPs nanocomposites (c)
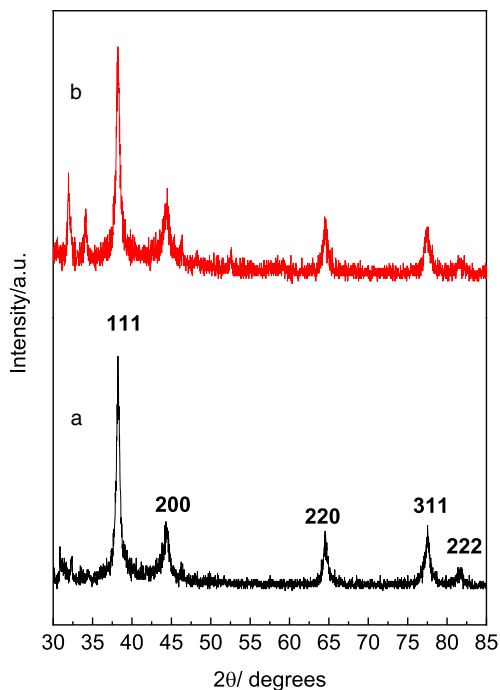
FIGURE 1 X-ray diffraction patterns of the silver nanoparticles (AgNPs) (a) and Cipro-AgNPs nanocomposites (b)
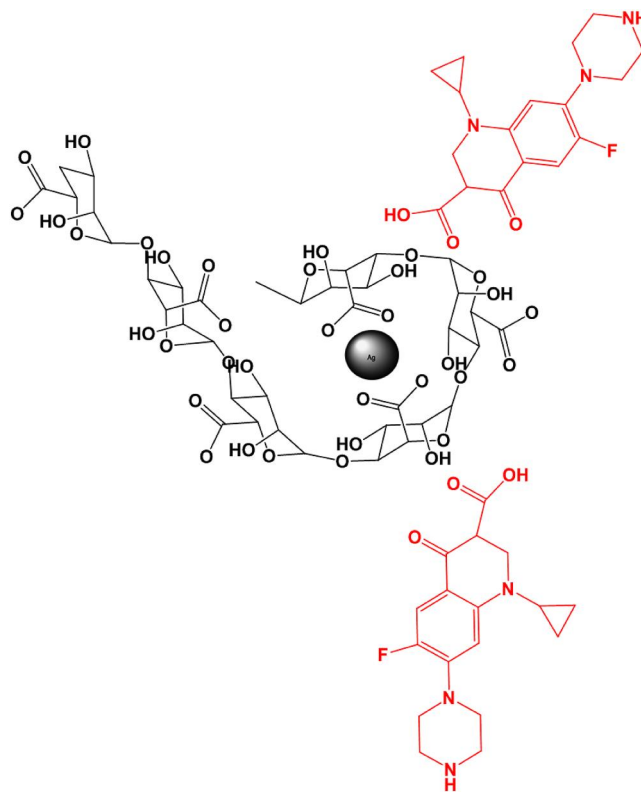
FIGURE 3 Possible interaction between Cipro, silver nanoparticles and alginate

(a)

(b)

(c)

F I G U R E 4   TGA curve showing free Cipro (a), silver nanoparticles (AgNPs), (b) and Cipro-AgNPs nanocomposites (c)

C–O and C–N bonds, while the peak at 1269 cm^{-1} represented bending of hydroxide group. The strong peak at 1039 cm^{-1} was assigned to the C–F group [32] (Figure 2a).

For AgNPs capped with alginate (Figure 2b), the FT-IR spectrum showed a peak at 3397 cm^{-1}, representing hydroxide and/or amine stretching [33]. The band shown at 2802 cm^{-1} was due to C–H alkane stretching. The small peak observed at 2136 cm^{-1} was due to the carbonyl stretching. The peak seen at 1618 cm^{-1} was due to the bending of the amine bond. The peaks shown at 1340 cm^{-1} and 1083 cm^{-1} were due to the C–H alkane bending and C–O alcohol/ether stretching, respectively [33, 34].

Matching the main peaks of the AgNPs with pure Cipro and Cipro-AgNPs nanocomposites, the results showed that there was interaction between Cipro and capped AgNPs. In the FT-IR spectrum in Figure 2c, the Cipro-AgNPs nanocomposites show a peak at 3388 cm^{-1} which was due to the stretching of hydroxide and hydrogen bonding, while the peak at 1035 cm^{-1} represented C–F stretching vibration.

Figure 3 shows the interactions between the three components of Cipro-AgNPs nanocomposites. The AgNPs capped by alginate throw a lone pair of electrons of oxygen around the Alg [35]. In addition, a hydrogen bond is seen in the type of interaction between Cipro and AgNPs in Cipro-AgNPs nanocomposites [36].

3.3 | Thermogravimetric analysis (TGA)

The thermal properties of the materials during incorporation of Cipro into AgNPs were determined using TGA and DTA analysis (Figure 4). The free Cipro seen in Figure 4a shows four mass losses steps. The first step occurred between 39 and 216°C with a mass loss of 4.2%, corresponding to the loss of acetylene molecule (C_2H_2) [37]. The second and third mass losses were seen between 216–356°C and 356–534°C at a maxima of 322°C and 410°C, respectively; these can be attributed to the loss of acetylene molecule (C_2H_2), ethylene (C_2H_4), mono nitrogen oxide (NO), hydrogen fluoride (HF) and hydrogen gas (H_2) [37].

TGA/DTG curves of AgNPs are given in Figure 4b. It can be seen from the figure that the dominant mass loss of the AgNPs occurred in the region between 171 and 878°C in two steps. These were due to the degradation of the polymer [38, 39].

TGA curves of the Cipro-AgNPs nanocomposites are given in Figure 4c. The figure shows that three mass losses occurred in the region between 30 and 878°C. The first mass loss was between 30°C and 171°C with 9.9% mass loss, due to the loss of the H_2O molecule. The second and third stages (overlapping steps) were due to the degradation of Cipro drug, formation of a carbonaceous residue and degradation of the polymer. In addition, TGA was used to analyse the amount of Cipro bound on the AgNPs, where the Cipro-AgNPs nanocomposites contained about 22% Cipro.
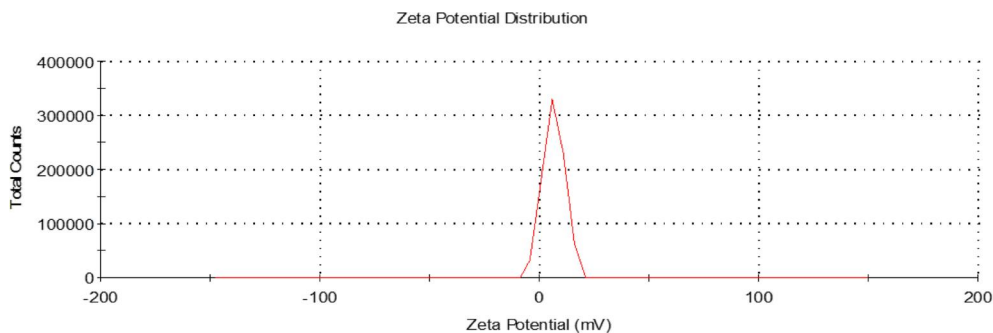
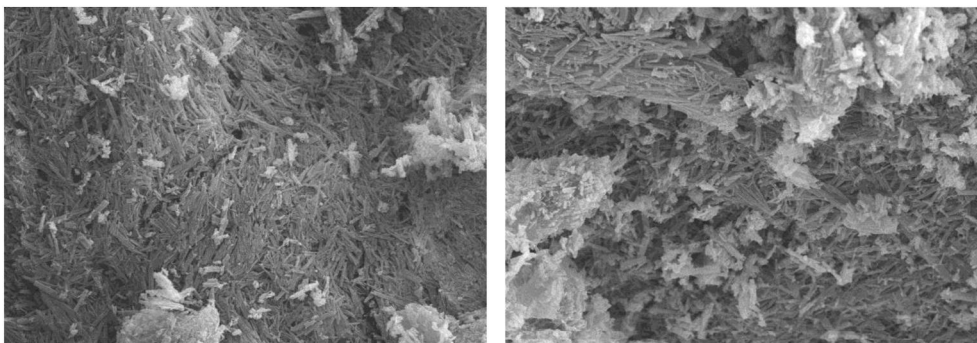**FIGURE 5** Zeta potential of Cipro-silver nanoparticles nanocomposites

FIGURE 6 SEM images of Cipro-silver nanoparticles nanocomposites
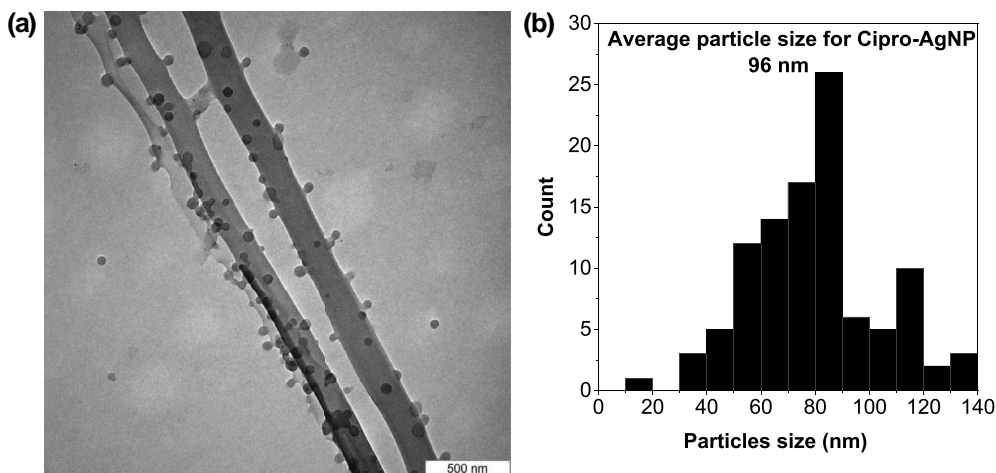

FIGURE 7 TEM image of Cipro-silver nanoparticles (AgNPs) nanocomposites (a), and the histogram of the Cipro-AgNPs nanocomposites size distribution (b)

3.4 | Zeta potential

The zeta potential instrument represents the stability of the nano-prepared particles in suspended media. Figure 5 shows the data of Cipro-AgNPs nanocomposites. The Cipro-AgNPs exhibited a positive zeta potential with a value of 6.5 mV.

3.5 | SEM analysis

SEM analysis was performed to study the morphological properties of Cipro-AgNPs nanocomposites (Figure 6). The SEM analysis revealed that particles were nearly round needle-lumpy shaped. Most of the Cipro-AgNPs nanocomposites were

aggregated, and very few individual Cipro-AgNPs nano-composites were also observed [40].

3.6 | Determination of the average size and size distribution

The TEM image of the Cipro-AgNPs nanocomposites is shown in Figure 7. It is evident that the Cipro-AgNPs nano-composites were mainly spherical in shape and well dispersed (Figure 7a). To determine the Cipro-AgNPs nanocomposites' size distribution, J Image software was used, and the data obtained was reported in a histogram (Figure 7b). The Cipro-AgNPs nanocomposites had an average size 96 nm.
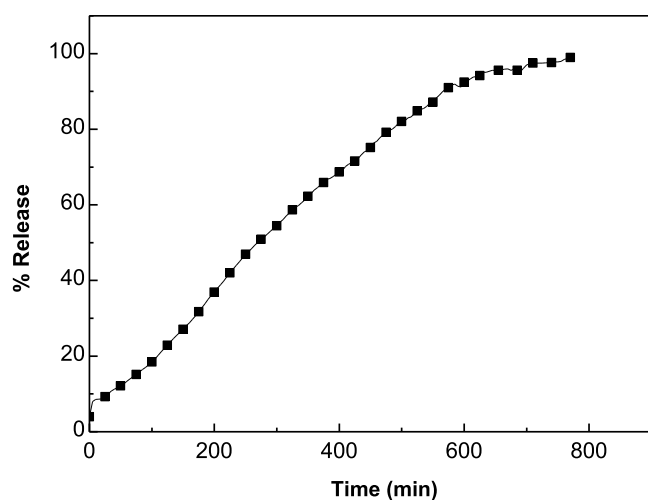
FIGURE 8 Cipro cumulative release percentage (%) profiles from Cipro-silver nanoparticles nanocomposite performed in phosphate buffered saline at pH 7.4

3.7 | Drug loading capacity and in vitro release study of Cipro from the Cipro-AgNPs nanocomposites

The calculated Cipro loading capacity by the UV instrument for prepared Cipro-AgNPs nanocomposites is 26.3% w/w. In vitro Cipro release tests from Cipro-AgNPs nanocomposites were performed at pH 7.4 to simulate intestinal fluid using phosphate buffered saline (PBS) medium. The percent of Cipro release profiles into the PBS medium versus time is shown in Figure 8. First, the Cipro release profiles indicate the presence of a burst of about 8.0% after 8 min. Then, the release from Cipro-AgNPs nanocomposites increases steeply, reaching 98% after 770 min. In this work, the first fast step of the release profile may be due to the release of the Cipro drug that is free on the surface of the AgNPs [41, 42]. The release in the slow second step is due to anion exchange between Cipro and phosphate anions in the release media. In addition, the release may be facilitated through the internal diffusion of AgNPs and Cipro anions.

The average dissolution time (ADST) is the average time required for drug dissolution. It is calculated according to Equation (2) [43].

$$\text{ADST}_{\text{in-vitro}} = \frac{\sum_{i=1}^{n} t_{mid}\Delta M}{\sum_{i=1}^{n} \Delta M} \tag{3}$$

where n is the number of dissolution times, ΔM is the concentration of the drug dissolved between time t_i and t_{i-1}, t_{min} is the time at midpoint between t and t_{j-1}, j term is the dissolution sample number.

A higher value of ADST indicates a higher drug withhold in the polymer and vice-versa [44]. The ADST value for Cipro-AgNPs nanocomposites was found to be 407.5 min; this result indicates a sustained release model.

T A B L E 1 The kinetics equations of the models used in fitting the Cipro drug release data from Cipro-silver nanoparticles nanocomposites [45–48]

Model	Equation	Parameters
Zero order	$q_t = k_0\,t$	K_0 is the zero-order rate constant
		q_t is the quantity released at any time (t)
		t is the time of drug release
Pseudo-first order	$\ln(q_e - q_t) = \ln q_e - k_1 t$	K_1 is the first-order rate constant
		q_e is the quantity released at equilibrium
Pseudo-second order	$t/q_t = 1/k_2 q_e^2 + t/q_e$	K_2 is the second-order rate constant
Higuchi	$q_t = K_H \sqrt{t}$	K_H is the Higuchi-order rate constant
Hixson–Crowell	$\sqrt[3]{M_o} - \sqrt[3]{q_t} = k_{H.C} t$	$K_{H.C}$ is the Hixson-Crowell-order rate constant
		M_o is the initial quantity of the drug in the nanocomposite
Korsmeyer–Peppas	$\frac{q_t}{q_\infty} = K_{k.p} t^n$	$K_{k.p}$ is the Korsmeyer-Peppas -order rate constant
		q_∞ is the release at infinite time

3.8 | Release kinetics of Cipro from the Cipro-AgNPs nanocomposites

The mechanism of Cipro release from Cipro-AgNPs nanocomposites was estimated using six models to fit the experimental cumulative drug release data (Table 1).

Cipro release kinetics from the Cipro-AgNPs nanocomposites is shown in Figure 9 with regression coefficient (R^2) values. From the figure, the release of Cipro from Cipro-AgNPs nanocomposites followed the Hixson–Crowell kinetic model with R^2 values of 0.9847.

The Hixson–Crowell law was also called the cube root equation. The equation describes the release from nanocomposites where there is a change in surface area and diameter of particles [49].

3.9 | Cytotoxicity studies

The cytotoxic effects of the Cipro, AgNPs and Cipro-AgNPs nanocomposites on the viability of the 3T3 cell lines are presented as percent cell viability in Figure 10. Values obtained
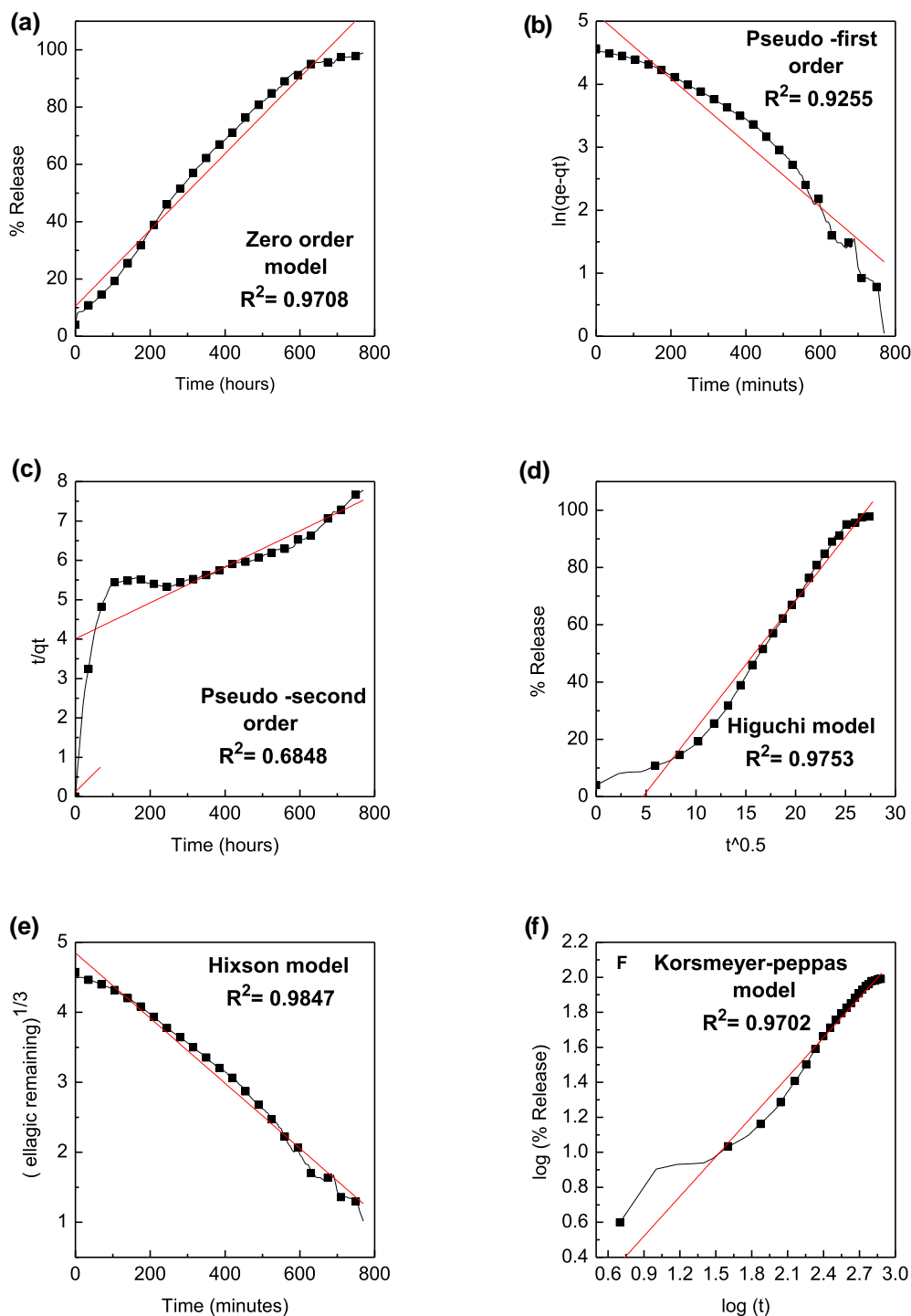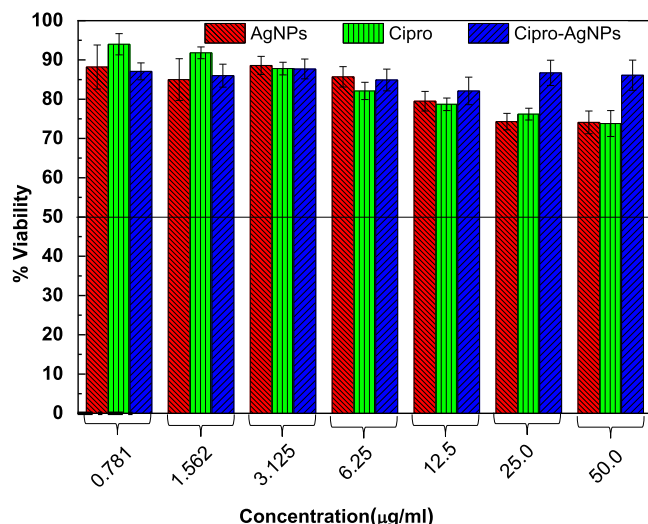

FIGURE 9 Release data fitting for Cipro release from Cipro-silver nanoparticles nanocomposites using six kinetic models

FIGURE 10 Cytotoxicity of the Cipro, silver nanoparticles (AgNPs) and Cipro-AgNPs nanocomposites after treatment of the 3T3 cell line

from MTT assays were calculated. As shown in Figure 10, there is no toxic effect in different concentrations of AgNPs and Cipro-AgNPs nanocomposites in 3T3 cells which indicates the nontoxic nature in normal cells [50].

4 | CONCLUSION

The preparation and characterisation of Cipro-AgNPs nanocomposites have been described in this work. From X-ray diffraction and Scherrer's equation, the average particle size was determined and found to be 100 nm which is agreed with the TEM result. The TGA study shows that the loading of Cipro in nanocomposites was 22% which agrees with the UV-Vis results. In addition, long time release of Cipro from nanocomposites followed the Hixson–Crowell kinetic model. The cytotoxicity study shows safety properties for nanocomposites, therefore they have potential applications in drug delivery.

CONFLICT OF INTEREST
The authors report no conflicts of interest in this work.

DATA AVAILABILITY STATEMENT
Research data are not shared.

ORCID
Samer Hasan Hussein-Al-Ali https://orcid.org/0000-0002-8760-6069

REFERENCES
1. Rizvi, S.A., Saleh, A.M.: Applications of nanoparticle systems in drug delivery technology. Saudi Pharmaceut. J. 26(1), 64–70 (2018)
2. Lenders, V., et al.: Biomedical nanomaterials for immunological applications: ongoing research and clinical trials. Nanoscale Adv. 2(11), 5046–5089 (2020)
3. Cobos, M., et al.: Graphene oxide–silver nanoparticle nanohybrids: synthesis, characterization, and antimicrobial properties. Nanomaterials 10(2), 376 (2020)
4. Jarai, B.M., et al.: Evaluating UiO-66 metal–organic framework nanoparticles as acid-sensitive carriers for pulmonary drug delivery applications. ACS Appl. Mater. Interfaces 12(35), 38989–39004 (2020)
5. Jung, D.S., et al.: Ultrasonic spray pyrolysis for air-stable copper particles and their conductive films. Acta Mater. 206, 116569 (2021)
6. Leong, K.H., et al.: Solar photocatalytic activity of anatase TiO_2 nanocrystals synthesized by non-hydrolitic sol–gel method. Sol. Energy 101, 321–332 (2014)
7. Mehta, T., et al.: Manufacturing techniques for carbon nanotubes, gold nanoparticles, and silver nanoparticles. In: Emerging Technologies for Nanoparticle Manufacturing, pp. 397–420. Springer, Berlin (2021)
8. Afolalu, S.A., et al.: Application of nanomaterials and nanotechnology in addressing Covid-19 challenges–review. In: 2nd South American Conference on Industrial Engineering and Operations Management, IEOM 2021, pp. 920–926 (2021)
9. Zhang, X.-F., et al.: Silver nanoparticles: synthesis, characterization, properties, applications, and therapeutic approaches. Int. J. Mol. Sci. 17(9), 1534 (2016)
10. Kim, S., Ryu, D.Y.: Silver nanoparticle-induced oxidative stress, genotoxicity and apoptosis in cultured cells and animal tissues. J. Appl. Toxicol. 33(2), 78–89 (2013)
11. Castangia, I., et al.: Combination of grape extract-silver nanoparticles and liposomes: a totally green approach. Eur. J. Pharmaceut. Sci. 97, 62–69 (2017)
12. Li, P., et al.: Green synthesis of β-CD-functionalized monodispersed silver nanoparticles with enhanced catalytic activity. Colloids Surf. A Physicochem. Eng. Asp. 520, 26–31 (2017)
13. Buszewski, B., et al.: Novel aspects of silver nanoparticles functionalization. Colloids Surf. A Physicochem. Eng. Asp. 506, 170–178 (2016)
14. Kaur, A., Goyal, D., Kumar, R.: Surfactant mediated interaction of vancomycin with silver nanoparticles. Appl. Surf. Sci. 449, 23–30 (2018)
15. Prasad, S.R., et al.: Formulation and evaluation of azathioprine loaded silver nanoparticles for the treatment of rheumatoid arthritis. AJBPS. 3(23), 28–32 (2013)
16. Sherwood, L., Kristin, W.: Development of ciprofloxacin: the USA perspective. In Ciprofloxacin: 10 Years of Clinical Experiences, pp. 1–5. Maxim Medical, Oxford (1997)
17. Singh, K., Mishra, A., Singh, A.: Synthesis characterization and in vitro release study of ciprofloxacin-loaded chitosan nanoparticle. Bionanoscience 8(1), 229–236 (2018)
18. Cartwright, A.C.: The British pharmacopoeia, 1864 to 2014: medicines, international standards and the state (2016)
19. Savjani, K.T., Gajjar, A.K., Savjani, J.K.: Drug solubility: importance and enhancement techniques. Int. Sch. Res. Not. 1–10 (2012)
20. Urquhart, A.J., Eriksen, A.Z.: Recent developments in liposomal drug delivery systems for the treatment of retinal diseases. Drug Discov. Today 24(8), 1660–1668 (2019)
21. Lingayat, V.J., Zarekar, N.S., Shendge, R.S.: Solid lipid nanoparticles: a review. Nanosci. Nanotechnol. Res. 2, 67–72 (2017)
22. Villanueva, J.R., Navarro, M.G., Villanueva, L.R.: Dendrimers as a promising tool in ocular therapeutics: latest advances and perspectives. Int. J. Pharm. 511(1), 359–366 (2016)
23. Mandal, A., et al.: Polymeric micelles for ocular drug delivery: from structural frameworks to recent preclinical studies. J. Contr. Release 248, 96–116 (2017)
24. Assali, M., et al.: Single-walled carbon nanotubes-ciprofloxacin nano-antibiotic: strategy to improve ciprofloxacin antibacterial activity. Int. J. Nanomed. 12, 6647–6659 (2017)

25. Sreedharan, S.M., Singh, R.: Ciprofloxacin functionalized biogenic gold nanoflowers as nanoantibiotics against pathogenic bacterial strains. Int. J. Nanomed. 14, 9905–9916 (2019)

26. Akbari, V., et al.: Ciprofloxacin nano-niosomes for targeting intracellular infections: an in vitro evaluation. J. Nanoparticle Res. 15(4), 1556 (2013)

27. Topal, G.R., et al.: Design of ciprofloxacin-loaded nano-and micro-composite particles for dry powder inhaler formulations: preparation, in vitro characterisation, and antimicrobial efficacy. J. Microencapsul. 35(6), 533–547 (2018)

28. Stockert, J.C., et al.: MTT assay for cell viability: intracellular localization of the formazan product is in lipid droplets. Acta Histochem. 114(8), 785–796 (2012)

29. Venkatesham, M., et al.: Synthesis of stable silver nanoparticles using gum acacia as reducing and stabilizing agent and study of its microbial properties: a novel green approach. Int. J. Green Nanotechnol. 4(3), 199–206 (2012)

30. Roy, K., Sarkar, C., Ghosh, C.: Plant-mediated synthesis of silver nanoparticles using parsley (Petroselinum crispum) leaf extract: spectral analysis of the particles and antibacterial study. Appl. Nanosci. 5(8), 945–951 (2015)

31. Scherrer, P.: Determination of the size and internal structure of colloidal particles using X-rays. Nachr. Ges. Wiss. Göttingen. 2, 98–100 (1918)

32. Tom, R.T., et al.: Ciprofloxacin-protected gold nanoparticles. Langmuir 20(5), 1909–1914 (2004)

33. Bhagyaraj, S., Krupa, I.: Alginate-mediated synthesis of hetero-shaped silver nanoparticles and their hydrogen peroxide sensing ability. Molecules 25(3), 435 (2020)

34. Huq, M.: Green synthesis of silver nanoparticles using Pseudoduganella eburnea MAHUQ-39 and their antimicrobial mechanisms investigation against drug resistant human pathogens. Int. J. Mol. Sci. 21(4), 1510 (2020)

35. Mandal, A., et al.: Vibrational spectroscopic investigation on interaction of sago starch capped silver nanoparticles with collagen: a comparative physicochemical study using FT-IR and FT-Raman techniques. RSC Adv. 5(21), 15763–15771 (2015)

36. Ma, J., et al.: Water-enhanced removal of ciprofloxacin from water by porous graphene hydrogel. Sci. Rep. 5(1), 1–10 (2015)

37. Sadeek, S.A., et al.: Spectroscopic, structure and antimicrobial activity of new Y (III) and Zr (IV) ciprofloxacin. Spectrochim. Acta Mol. Biomol. Spectrosc. 78(2), 854–867 (2011)

38. Rescignano, N., et al.: Preparation of alginate hydrogels containing silver nanoparticles: a facile approach for antibacterial applications. Polym. Int. 65(8), 921–926 (2016)

39. Valentini, L., et al.: Preparation of alginate/graphene oxide hybrid films and their integration in triboelectric generators. Eur. J. Inorg. Chem. 7(0), 1192–1197 (2015)

40. Rautela, A., Rani, J., Das, M.D.: Green synthesis of silver nanoparticles from Tectona grandis seeds extract: characterization and mechanism of antimicrobial action on different microorganisms. J. Anal. Sci. Technol. 10(1), 1–10 (2019)

41. Su, Z., et al.: Chitosan/silver nanoparticle/graphene oxide nano-composites with multi-drug release, antimicrobial, and photothermal conversion functions. Materials 14(9), 2351 (2021)

42. Gomes, H.I., Martins, C.S., Prior, J.A.: Silver nanoparticles as carriers of anticancer drugs for efficient target treatment of cancer cells. Nano-materials. 11(4), 964 (2021)

43. Möckel, J.E., Lippold, B.C.: Zero-order drug release from hydrocolloid matrices. Pharm. Res. (N. Y.) 10(7), 1066–1070 (1993)

44. Roni, M., Kibria, G., Jalil, R.: Formulation and in vitro evaluation of alfuzosin extended release tablets using directly compressible eudragit. Indian J. Pharmaceut. Sci. 71(3), 252 (2009)

45. Dong, L., et al.: Synthesis and release behavior of composites of camptothecin and layered double hydroxide. J. Solid State Chem. 183(8), 1811–1816 (2010)

46. Ho, Y.-S., Ofomaja, A.E.: Pseudo-second-order model for lead ion sorption from aqueous solutions onto palm kernel fiber. J. Hazard Mater. 129(1), 137–142 (2006)

47. Sakore, S., Chakraborty, B.: Formulation and evaluation of enalapril maleate sustained release matrix tablets. Int. J. Pharm. 4(1), 21–26 (2013)

48. Brouers, F., Al-Musawi, T.J.: The use of the Brouers–Sotolongo fractal kinetic equation for the study of drug release. Adsorption. 26(6), 843–853 (2020)

49. Paarakh, M.P., et al.: Release kinetics—concepts and applications. Int J Pharm Res Technol. 8(1), 12–20 (2018)

50. Singh, P., et al.: Pharmacological importance, characterization and applications of gold and silver nanoparticles synthesized by Panax ginseng fresh leaves. Artif. Cell. Nanomed. Biotechnol. 45(7), 1415–1424 (2017)